Mitochondrial Colocalization with Ca^{2+} Release Sites is Crucial to Cardiac Metabolism

Asuka Hatano,* Jun-ichi Okada, Takumi Washio, Toshiaki Hisada, Seiryo Sugiura

Department of Frontier Science, The University of Tokyo, Kashiwa, Chiba, Japan

Submitted July 13, 2012, and accepted for publication December 4, 2012.

*Correspondence: asuka-h@sml.k.u-tokyo.ac.jp

SUPPLEMENTAL METHODS

1 Three-dimensional finite element mesh of cardiomyocyte

Fig. S1 shows the structure of a 3D model of the myocyte (CTR model). To reduce the computational cost, we modeled a segment containing only three myofibrils of one sarcomere length, together with the adjacent cell membrane and organelle (Fig. S1, left panel). The rationale behind such modeling is the longitudinal periodicity and axial symmetry of the myocyte. We assumed a cylindrical myocyte containing 40 myofibrils, and three radially arranged myofibrils occupied the space between the cell membrane and the center of the myocyte. At the final stage, further reductions were implemented to include only one quarter of this model for analysis (halved in both length and width). The 3D structure was modeled with a hexahedral solid finite element.

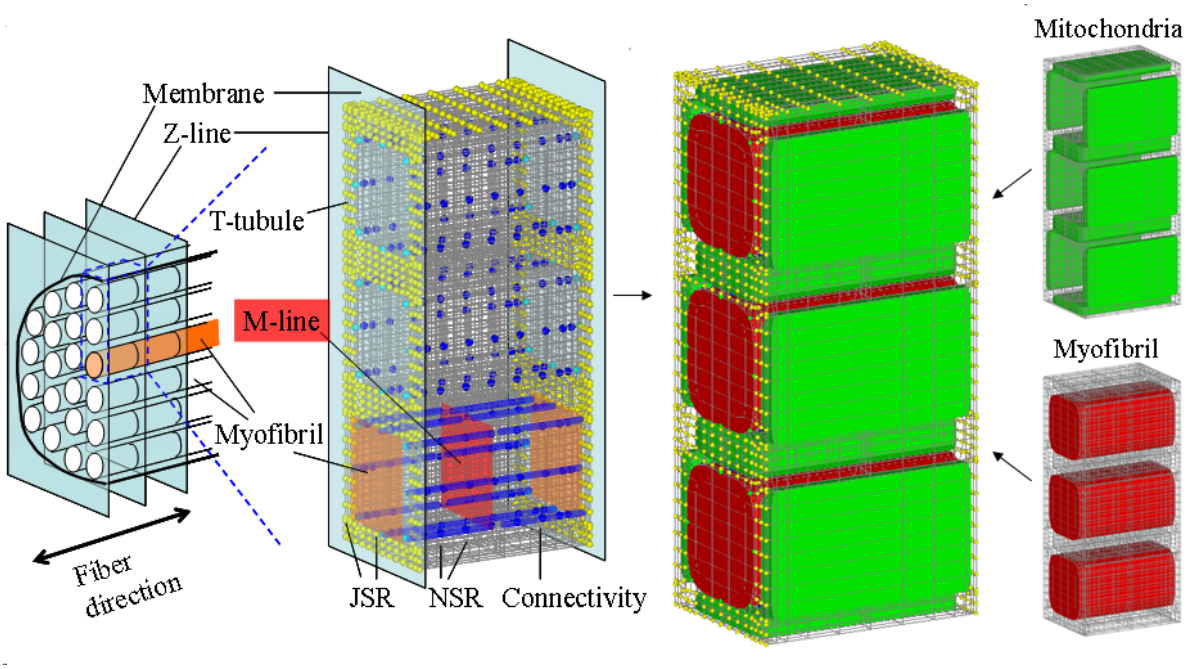

Figure S 1: Finite element mesh

1.1 Mesh construction

Construction of mesh that is sufficiently fine to reproduce every detail of the subcellular component is impractical. Therefore, first, we constructed a mesh expressing the three major volume fractions, namely, the myofibril, mitochondrion, and the remaining components. The cytosolic reaction-diffusion field was defined in the whole mesh. Second, small subcellular components were located at the appropriate nodes

to reproduce the anatomical structure. These subcellular components shared their fractional volumes as double nodes. Fig. S1 shows the constructed mesh in which The JSR node is shown in light blue, the NSR node is shown in blue, the membrane and t-tubule node are shown in yellow, mitochondria are shown in green, myofibril is shown in red, and other structures are transparent. The second left panel shows Ca^{2+} transport pathways from the NSR to JSR. In the right panels, the model is decomposed to show the distribution of myofibril and mitochondria in the 3D structure of the whole model.

The functional volume of each node was defined by finite-element integration of the volume of functional elements such as myofibrils, mitochondria, and the cytosol. Uptake and release by the subcellular components are expressed as the flux between the functional volumes at the node.

Finally, to investigate the effect of the gap between the JSR Ca^{2+} release site and mitochondria, mesh near the gap was finer. The model consisted of 1861 nodes and 581 elements. The total number of degrees of freedom was 6164 for mechanical analysis and approximately 20,000 for reaction-diffusion simulation.

2 Reaction-diffusion equations

2.1 Governing Equations

Numerical studies have investigated Ca^{2+} dynamics in 3D space with reaction-diffusion equations [1, 2, 3, 4]. The current study adopted these formulas for calculating the transport and exchange of metabolites, ions, and signaling molecules (substrates). The multiple reaction-diffusion fields for six substrates, namely Ca^{2+}, creatine (Cr), creatine phosphate (CP), inorganic phosphate (Pi), adenosine tri-phosphate (ATP) and adenosine di-phosphate (ADP) were defined in the cytosolic space as follows.

$$\frac{\partial c_i^\alpha}{\partial t} = \boldsymbol{\nabla} \cdot (\boldsymbol{D}_i^\alpha \boldsymbol{\nabla} c_i^\alpha) + f_i^\alpha(\boldsymbol{c}_i) \tag{1}$$

Here, α indicates each of the six substrates, i indicates the location, $\boldsymbol{D}^\alpha$ is a diagonal matrix containing the diffusivity of the substrate α, c^α is the concentration of the substrate α, and f_i^α is the function describing the reaction involving the substrate α at the loci i dependent on all the substrates concentrations $\boldsymbol{c}_i$. We adopted the functional forms from the model by Cortassa et al. [5]. Details of functional forms will be described in section 4. The diffusion coefficients used in this study are shown in Table S1.

We solved the reaction-diffusion equations of Ca^{2+} inside the mitochondrial matrix separately because a significant gradient is expected. The mitochondrial inner membrane potential was shared by all the nodes in a mitochondrion. Considering the dense structure of cristae in cardiac mitochondria, we reduced the diffusion coefficient to 1/100 of the cytosol.

Substrate	axial $\boldsymbol{D}$	transverse $\boldsymbol{D}$	reference
Ca^{2+}	0.300	0.1880	[2, 3, 4, 7]
Cr	0.149	0.0936	[6, 7]
CP	0.114	0.0713	[6, 7]
Pi	0.140	0.0877	[6, 7]
ADP	0.078	0.0490	[6, 7]
ATP	0.083	0.0520	[6, 7]

Table S 1: Diffusion coefficients

3 Mechanical simulation

The cardiomyocyte is composed of multiple subcellular components, each having distinct material properties in terms of the stress-strain relationship and bulk modulus. Furthermore, the excitation-contraction mechanism introduces time-varying anisotropic stiffness in the myofibril, which in turn creates a heterogeneous force field in the cellular space. To treat such a complex object in a unified way, we needed to apply a mixed finite element method based on the perturbed Lagrange-multiplier method. The governing equations are:

$$\int_V \left(2\frac{\partial W}{\partial \boldsymbol{C}} + \lambda J \boldsymbol{C}^{-1}\right) : \delta \boldsymbol{E} dV + \int_{S_t} \tilde{\boldsymbol{t}}_b \cdot \delta \boldsymbol{u} dS = 0 \tag{2}$$

$$\int_V \delta\lambda \left\{(J-1) - \frac{2\lambda}{\kappa}\right\} dV = 0 \tag{3}$$

where W denotes strain energy function, $\boldsymbol{C}$ denotes right Cauchy-Green deformation tensor, J denotes volume change ($J = 1/2det(\boldsymbol{C})$)

$\boldsymbol{E}$ denotes Green-Lagrange strain tensor, $\boldsymbol{S}$ denotes second Piola-Kirchhoff stress tensor (with assumption of hyper-elastisity, $\boldsymbol{S} = 2\frac{\partial \boldsymbol{W}}{\partial \boldsymbol{C}}$), $\boldsymbol{u}$ is displacement, λ is a Lagrange multiplier for volumetric constraint (corresponding to $-\frac{1}{2}$ of the pressure), V is analysis volume, κ is bulk modulus, $\tilde{\boldsymbol{t}}_b$ is the stress boundary condition, and S_t is the surface where the stress boundary condition is defined.

Eq. (2) is the equilibrium equation and eq. (3) is the compressibility control condition. We solved eqns. (2) and (3), which are nonlinear equations of two variables ($\boldsymbol{u}$,λ), by using finite element methods.

3.1 Constitutive equation for mitochondria and other components

Mitochondria and other intracellular components excluding myofibrils were regarded as isotropic soft tissue. The following constitutive equation for Mooney-Rivlin material using reduced invariants was applied.

$$W = c_1(\tilde{I}_1 - 3) + c_3(\tilde{I}_1 - 3)^2 + c_7(\tilde{I}_1 - 3)^2(\tilde{I}_2 - 3)$$

where $\tilde{I}_i$ is i^{th} reduced invariants of $\boldsymbol{C}$. We used parameters in Table S2, which were fitted for biomaterials [13].

Table S 2: Constants of Mooney-Rivlin material[13]unit(N/μm^2)

c_1	c_3	c_7
0.7×10^{-11}	0.32×10^{-9}	0.7×10^{-11}

3.2 Constitutive equation for myofibrils

To characterize the time-varying material properties of myofibrils, we adopted a constitutive equation for myocardium described by Watanabe et al.[13], which combines the passive property model by Humphrey et al. [14] and the active property model by Lin and Yin. [15]. Parameters were modified according to the experimental data of a single myofibril by Linke et al. [16]and Akiyama et al. [17] The strain-energy function of myofibrils is expressed as a sum of a passive part (W_p) and an active part (W_a) as follows and the parameters of the active part are the functions of activation level Fr:

$$\alpha = \sqrt{I_4} \tag{4}$$

$$W = W_p + W_a \tag{5}$$

$$W_p = c_{p1}(\alpha-1)^2 + c_{p2}(\alpha-1)^3 + c_{p3}(I_1-3) + c_{p4}(I_1-3)(\alpha-1) + c_{p5}(I_1-3)^2 \tag{6}$$

$$W_a = c_{a0} + c_{a1}(I_1-3)(I_4-1) + c_{a2}(I_1-3)^2 + c_{a3}(I_4-1)^2 + c_{a4}(I_1-3) \tag{7}$$

where $c_{a0} = c_{a00}F_r$, $c_{a1} = c_{a10}F_r$, $c_{a2} = c_{a20}F_r$, $c_{a3} = c_{a30}F_r$, $c_{a4} = c_{a40}F_r^2$, and Fr: normalized force for the activation level $F_r = force/force_{\max}$, $force_{\max}$= 0.1 N mm^{-2}.

Table S 3: Constants of myofibril model (N/μm^2)

c_{p1}	c_{p2}	c_{p3}	c_{p4}	c_{p5}
12.32×10^{-9}	12.96×10^{-9}	2.872×10^{-9}	-7.76×10^{-9}	6.64×10^{-9}
c_{a0}	c_{a1}	c_{a2}	c_{a3}	c_{a4}
3.08×10^{-9}	3.24×10^{-9}	0.359×10^{-9}	-1.94×10^{-9}	3.32×10^{-9}

4 Reaction term of each subcellular component

Equations and parameter values are from Cortassa et al. [5], except for the values with remarks and comments.

4.1 General parameters

F	96.5	C/mmol	Faraday constant.
T	310	K	Absolute temperature.
R	8.314	J $\mathrm{mol}^{-1}\mathrm{K}^{-1}$	Universal gas constant.

$$\begin{aligned}
\sum_{\text{membrane}} \text{area} &= \sum_{\text{t-tubule}} \text{area} = 7.5 \times 10^{-9}\ cm^2 \\
\sum \text{vol}_{\text{cyto}} &= 3.375\ nL\ (100.00\ \%) \\
\sum \text{vol}_{\text{mito}} &= 1.174\ nL\ (\ 34.70\ \%) \\
\sum \text{vol}_{\text{myo}} &= 1.819\ nL\ (\ 53.9\ \%) \\
\sum \text{vol}_{\text{JSR}} &= 1.114\ pL\ (\ \ 0.033\%) \\
\sum \text{vol}_{\text{NSR}} &= 0.103\ nL\ (\ \ 3.05\ \%)
\end{aligned}$$

where $\sum_{***}$area means the sum of the area, which belong to $***$, and $\sum \text{vol}_{***}$ means the sum of the volume, which belong to $***$.

4.2 Cytosolic reaction

Reaction terms of cytosol f_{cyto} become:

$$f^{\text{ADP}}_{\text{cyto}} = -f^{\text{ATP}}_{\text{cyto}} = +V_{\text{CK}} + V_{\text{cytATPase}} \tag{8}$$

$$f^{\text{Cr}}_{\text{cyto}} = -f^{\text{CP}}_{\text{cyto}} = -V_{\text{CK}} \tag{9}$$

$$f^{\text{Pi}}_{\text{cyto}} = +V_{\text{cytATPase}} \tag{10}$$

V_{CK} is creatine kinase reaction and $V_{\text{cytATPase}}$ is basal metabolism. These parameters are described later in this section.

Cytosolic $\mathbf{Ca^2}$+buffer Cytosolic Ca^{2+} buffer affects Ca^{2+} dynamics. The reaction-diffusion equation was modified to include this effect.

$$\frac{\partial[\text{Ca}^{2+}]_{\text{cyto}}}{\partial t} = \left(1 + \frac{K^{\text{cyto}}_{\text{CMDN}}[CMDN]^{\text{cyto}}_{\text{tot}}}{(K^{\text{cyto}}_{\text{CMDN}} + [Ca^{2+}]_{\text{cyto}})^2}\right)^{-1} (D^{\text{Ca}^{2+}}\nabla^2[Ca^{2+}]_{\text{cyto}} + f^{\text{Ca}^{2+}}) \tag{11}$$

Creatine kinase reaction Creatine kinase reactions are present in the cytosol, which is colocalized with mitochondria, the M-line, NSR, and membrane.

$$V_{\text{CK}} = k^{***}_{\text{CK}}\left([\text{ATP}][\text{Cr}] - \frac{[\text{ADP}][\text{CP}]}{K_{\text{eq}}}\right) \tag{12}$$

where $***$ denotes either mitochondria, M-line, NSR, or membrane.

Basal metabolism The basal cytosolic ATP consumption rate was assumed to be homogeneous throughout the cytoplasm.

$V_{\mathrm{cytATPase}} = 1.0 \times 10^{-5}$ [mM/ms]

parameter	value	unit	reference
$K_{\mathrm{CMDN}}^{\mathrm{cyto}}$	2.38×10^{-3}	mM	[5]
$[\mathrm{CMDN}]_{\mathrm{tot}}^{\mathrm{cyto}}$	5.0×10^{-2}	mM	[5]
K_{eq}	0.0095		[22]*
$k_{\mathrm{CK}}^{\mathrm{mito}}$	6.67×10^{-5}	mmol $\mathrm{L}^{-1}\mathrm{ms}^{-1}$	[5]**
$k_{\mathrm{CK}}^{\mathrm{Mline}}$	7.0×10^{-3}	mmol $\mathrm{L}^{-1}\mathrm{ms}^{-1}$	[5]**
$k_{\mathrm{CK}}^{\mathrm{NSR}}$	7.0×10^{-3}	mmol $\mathrm{L}^{-1}\mathrm{ms}^{-1}$	[5]**
$k_{\mathrm{CK}}^{\mathrm{membrane}}$	7.0×10^{-3}	mmol $\mathrm{L}^{-1}\mathrm{ms}^{-1}$	[5]**

Table S 4: Constants for cytosolic reactions

* K_{eq} was estimated from data by Johannes H.G.M. van Beek [22].

** CK is condensed more than 10 times into mitochondria or the cytosolic space near subcellular components. This induces a high local concentration of metabolites and inhibits CK. To maintain energy metabolite level and flux, the value of k_{CK} was increased to 50 times.

4.3 Membrane and t-tubules

Ion channel distributions on peripheral and t-tubule membranes were included in the model, as reported by Pasek et al. [23]. Distributions are defined as distributions of permeability of the channel per unit membrane area, and are shown in Table S5. Because our model is primarily based on the Cortassa model, total channel permeability was defined in a manner consistent with the Cortassa model. At the Ca^{2+} release site, channel distribution is different from other regions of the t-tubule membrane, and only the LCC is clustered without other ion channels.

The membrane potential is uniform throughout the model as shown in the following eq. 16, because an experimental study suggested that the whole cell membrane is electrically well coupled [24].

Reaction terms at the membrane or t-tubule node f_{mbr} become:

$$f_{\mathrm{mbr}}^{\mathrm{Ca^{2+}}} = -I_{\mathrm{Ca_{tot}}} \frac{\mathrm{area}}{2\mathrm{vol}_{\mathrm{cyto}} F} \tag{13}$$

$$f_{\mathrm{mbr}}^{\mathrm{ADP}} = +(I_{\mathrm{pCa}} + I_{\mathrm{NaK}}) \frac{\mathrm{area}}{\mathrm{vol}_{\mathrm{cyto}} F} \tag{14}$$

$$f_{\mathrm{mbr}}^{\mathrm{ATP}} = -(I_{\mathrm{pCa}} + I_{\mathrm{NaK}}) \frac{\mathrm{area}}{\mathrm{vol}_{\mathrm{cyto}} F} \tag{15}$$

where area denotes the functional membrane area, $\mathrm{vol}_{\mathrm{cyto}}$ denotes functional cytosolic volume, and F is the Faraday constant. $I_{\circ}$ denotes membrane current, and this is described later in this section.

The following variables were lumped in the model: sarcoplasmic membrane voltage (V), cytosolic

Na^+ and K^+ concentrations ([Na] and [K])

$$\frac{\mathrm{d[V]}}{\mathrm{d}t} = -\frac{1}{C_m}\frac{\sum_{\mathrm{cell}} I_{\mathrm{total}}\mathrm{area}}{\sum_{\mathrm{cell}}\mathrm{area}} \tag{16}$$

$$\frac{\mathrm{d[Na]}}{\mathrm{d}t} = -\frac{\sum_{\mathrm{cell}} I_{Na_{tot}}\mathrm{area}}{\sum_{\mathrm{cell}}\mathrm{vol}_{\mathrm{cyto}}F} \tag{17}$$

$$\frac{\mathrm{d[K]}}{\mathrm{d}t} = -\frac{\sum_{\mathrm{cell}} I_{K_{tot}}\mathrm{area}}{\sum_{\mathrm{cell}}\mathrm{vol}_{\mathrm{cyto}}F} \tag{18}$$

where

$$I_{\mathrm{total}} = I_{\mathrm{Na_{tot}}} + I_{\mathrm{K_{tot}}} + I_{\mathrm{Ca_{tot}}} \tag{19}$$

$$I_{\mathrm{Na_{tot}}} = I_{\mathrm{Na}} + I_{\mathrm{Na,b}} + I_{\mathrm{Ca(Na)}} + I_{\mathrm{ns(Na)}} + 3\times I_{\mathrm{NaK}} + 3\times I_{\mathrm{NaCa}} \tag{20}$$

$$I_{\mathrm{K_{tot}}} = I_{\mathrm{K}} + I_{\mathrm{K1}} + I_{\mathrm{Kp}} + I_{\mathrm{CaK}} + I_{\mathrm{ns(K)}} - 2\times I_{\mathrm{NaK}} \tag{21}$$

$$I_{\mathrm{Ca_{tot}}} = I_{\mathrm{Ca}} + I_{\mathrm{Ca,b}} + I_{\mathrm{p(Ca)}} - 2\times I_{\mathrm{NaCa}} \tag{22}$$

I_{Na} : Fast Na current (μA/μF)
I_{K} : Time-dependent delayed rectifier K current (μA/μF)
I_{K1} : Time-independent K current (μA/μF)
I_{Kp} : Plateau K current (μA/μF)
I_{NaK} : Na K pump current (μA/μF)
I_{NaCa} : NaCa exchanger current (μA/μF)
$I_{\mathrm{p(Ca)}}$: Sarcolemmal Ca pump current (μA/μF)
$I_{\mathrm{ns,K}}$: Non-specific Ca-activated K current (μA/μF)
$I_{\mathrm{Ca,b}}$: Ca background current (μA/μF)
$I_{\mathrm{Na,b}}$: Na background current (μA/μF)
I_{Ca} : Ca current through LCCs (μA/μF)
$I_{\mathrm{Ca,K}}$: K current through LCCs (μA/μF)

Fast Na current

$$I_{\mathrm{Na}} = \bar{G}_{\mathrm{Na}}\cdot m^3\cdot h\cdot j\cdot(V-E_{\mathrm{Na}}) \tag{23}$$

$$E_{\mathrm{Na}} = \frac{RT}{F}\cdot\ln\left(\frac{[\mathrm{Na}^+]_o}{[\mathrm{Na}^+]}\right) \tag{24}$$

$$\frac{dm}{dt} = \alpha_m(1-m)-\beta_m m \tag{25}$$

$$\frac{dh}{dt} = \alpha_h(1-h)-\beta_h h \tag{26}$$

$$\frac{dj}{dt} = \alpha_j(1-j)-\beta_j j \tag{27}$$

$$\alpha_m = 0.32\frac{(V+47.13)}{1-\mathrm{e}^{-0.1(V+47.13)}} \tag{28}$$

$$\beta_m = 0.08\mathrm{e}^{-V/11} \tag{29}$$

$$
\begin{aligned}
\textbf{\textit{For}} \quad & V \geq -40\text{mV} \\
\alpha_h &= \alpha_j = 0.0, && (30)\\
\beta_h &= (0.13(1+\mathrm{e}^{-(V+10.66)/11.1}))^{-1} && (31)\\
\beta_j &= 0.3 \cdot \frac{\mathrm{e}^{(-2.535\cdot 10^{-7}V)}}{1+\mathrm{e}^{-0.1(V+32)}} && (32)\\
\textbf{\textit{For}} \quad & V < -40\text{mV} \\
\alpha_h &= 0.135 \cdot \mathrm{e}^{(80+V)/-6.8} && (33)\\
\beta_h &= 3.56\mathrm{e}^{0.079V} + 3.1\times 10^5 \mathrm{e}^{0.35V} && (34)\\
\alpha_j &= [-1.2714\times 10^5 \mathrm{e}^{0.2444V} - 3.474\times 10^{-5}\mathrm{e}^{-0.04391V}] \times \frac{(V+37.78)}{1+\mathrm{e}^{0.311(V+79.23)}} && (35)\\
\beta_j &= 0.1212\frac{\mathrm{e}^{-0.01052V}}{1+\mathrm{e}^{-0.1378(V+40.14)}} && (36)
\end{aligned}
$$

E_{Na} : Reversal potential of Na (mV)

$\bar{G}_{\mathrm{Na}}$: Maximum conductance of the Na channel (mS/μF)

m : Na channel activation gate

h : Na channel inactivation gate

j : Na channel inactivation gate

Time-dependent delayed rectifier K current

$$
\begin{aligned}
I_{\mathrm{K}} &= \bar{G}_{\mathrm{K}} \cdot X_1 \cdot X^2 \cdot (V - E_{\mathrm{K}}) && (37)\\
E_{\mathrm{K}} &= \frac{RT}{F}\ln\left(\frac{[\mathrm{K}^+]_o + P_{\mathrm{Na,K}}[\mathrm{Na}^+]_o}{[\mathrm{K}^+] + P_{\mathrm{Na,K}}[\mathrm{Na}^+]}\right) && (38)\\
\bar{G}_{\mathrm{K}} &= 0.282\sqrt{\frac{[\mathrm{K}^+]_o}{5.4}} && (39)\\
X_1 &= (1+\mathrm{e}^{(V-40)/40})^{-1} && (40)\\
\frac{dX}{dt} &= \alpha_\chi(1-X) - \beta_\chi X && (41)\\
\alpha_\chi &= 7.19\times 10^{-5}\frac{V+30}{1-\mathrm{e}^{-0.148(V+30)}} && (42)\\
\beta_\chi &= 1.31\times 10^{-4}\frac{V+30}{-1+\mathrm{e}^{-0.0687(V+30)}} && (43)
\end{aligned}
$$

$\bar{G}_{\mathrm{K}}$: Channel conductance of time-dependent delayed rectifier K current (mS/μF)

X : Slowly activating K time-dependant activation

X_1 : Slowly activating K time-dependant activation

E_{Ks} : Reversal potential of time-dependent rectifier K current (mV)

$P_{\mathrm{Na,K}}$: Na/K permeability ratio

Time-independant K current

$$
\begin{aligned}
I_{\mathrm{K_1}} &= \bar{G}_{\mathrm{K_1}} \cdot K_{1\infty} \cdot (V - E_{\mathrm{K_1}}) && (44)\\
E_{\mathrm{K_1}} &= \frac{RT}{F} \cdot \ln\left(\frac{[\mathrm{K^+}]_o}{[\mathrm{K^+}]}\right) && (45)\\
\bar{G}_{\mathrm{K1}} &= 0.75 \cdot \sqrt{\frac{[\mathrm{K^+}]_o}{5.4}} && (46)\\
K_{1\infty} &= \frac{\alpha_{\mathrm{K_1}}}{\alpha_{\mathrm{K_1}} + \beta_{\mathrm{K_1}}} && (47)\\
\alpha_{\mathrm{K_1}} &= 1.02\left(1 + \mathrm{e}^{0.2385(V - E_{\mathrm{K_1}} - 59.215)}\right)^{-1} && (48)\\
\beta_{\mathrm{K_1}} &= \frac{0.4912\mathrm{e}^{0.08032(V - E_{\mathrm{K_1}} - 5.476)} + \mathrm{e}^{0.06175(V - E_{\mathrm{K_1}} - 594.31)}}{1 + \mathrm{e}^{-0.5143(V - E_{\mathrm{K_1}} + 4.753)}} && (49)
\end{aligned}
$$

$E_{\mathrm{K_1}}$: Reversal potential of time-independent K current (mV)
$\bar{G}_{\mathrm{K_1}}$: Channel conductance of time-independent K current (mS/μF)
$K_{1\infty}$: K inactivation

Plateau $\mathrm{K^+}$ current

$$
\begin{aligned}
I_{\mathrm{Kp}} &= \bar{G}_{\mathrm{K_p}} \cdot K_p (V - E_{\mathrm{K_p}}) && (50)\\
E_{\mathrm{Kp}} &= E_{\mathrm{K1}} && (51)\\
K_p &= \left(1 + \mathrm{e}^{(7.488 - V)/5.98}\right)^{-1} && (52)
\end{aligned}
$$

$\bar{G}_{\mathrm{K_p}}$: Channel conductance of plateau K current (mS/μF)
E_{Kp} : Reversal potential of plateau K current (mV)
K_p : K plateau factor

$\mathrm{Na^+}$-$\mathrm{Ca^{2+}}$ exchanger current

$$
I_{\mathrm{NaCa}} = k_{\mathrm{NaCa}} \frac{\mathrm{e}^{\eta \frac{VF}{RT}} [\mathrm{Na^+}]^3 \cdot [\mathrm{Ca^{2+}}]_o - \mathrm{e}^{(\eta - 1)\frac{VF}{RT}} [\mathrm{Na^+}]_o^3 \cdot [\mathrm{Ca^{2+}}]_{\mathrm{cyto}}}{(K_{\mathrm{m,Na}}^3 + [\mathrm{Na^+}]_o^3)(K_{\mathrm{m,Ca}} + [\mathrm{Ca^{2+}}]_o)(1 + k_{\mathrm{sat}} \mathrm{e}^{(\eta - 1)\frac{VF}{RT}})} \quad (53)
$$

$\mathrm{Na^+}$-$\mathrm{K^+}$ pump current

$$
\begin{aligned}
I_{\mathrm{NaK}} &= \bar{I}_{\mathrm{NaK}} \cdot f_{\mathrm{NaK}} \cdot f_{\mathrm{NaK}}^{\mathrm{ATP}} \cdot \frac{1}{1 + (K_{\mathrm{m,Nai}}/[\mathrm{Na^+}])^{1.5}} \cdot \frac{[\mathrm{K^+}]_o}{[\mathrm{K^+}]_o + K_{\mathrm{m,Ko}}} && (54)\\
f_{\mathrm{NaK}} &= \left(1 + 0.1245\mathrm{e}^{-0.1\frac{VR}{RT}} + 0.0365\mathrm{e}^{-\frac{VF}{RT}}\left(\frac{\mathrm{e}^{\frac{[\mathrm{Na^+}]_o}{67.3}} - 1}{7}\right)\right)^{-1} && (55)\\
f_{\mathrm{NaK}}^{\mathrm{ATP}} &= \left(1 + \frac{K_{\mathrm{1,NaK}}^{\mathrm{ATP}}}{[\mathrm{ATP}]_{\mathrm{cyto}}}\left(1 + \frac{[\mathrm{ADP}]_{\mathrm{cyto}}}{K_{\mathrm{i,NaK}}^{\mathrm{ADP}}}\right)\right)^{-1} && (56)
\end{aligned}
$$

$\bar{I}_{\mathrm{NaK}}$: Maximum current through the NaK pump (μA/μF)
$K_{\mathrm{m,Nai}}$: Na Half saturation concentration for the NaK pump (mM)
$K_{\mathrm{m,Ko}}$: K Half saturation concentration for the NaK pump (mM)
f_{NaK} : Voltage-dependence parameter of I_{NaK}
$f_{\mathrm{NaK}}^{\mathrm{ATP}}$: ATP and ADP dependence of I_{NaK}

Nonspecific Ca^{2+}-activated current

$$I_{\mathrm{ns(Ca)}} = I_{\mathrm{ns(K)}} + I_{\mathrm{ns(Na)}} \tag{57}$$

$$I_{\mathrm{ns(K)}} = \bar{I}_{\mathrm{ns(K)}} \cdot \frac{1}{1 + (K_{\mathrm{m,ns(Ca)}}/[\mathrm{Ca}^{2+}]_{\mathrm{cyto}})^3} \tag{58}$$

$$I_{\mathrm{ns(Na)}} = \bar{I}_{\mathrm{ns(Na)}} \cdot \frac{1}{1 + (K_{\mathrm{m,ns(Ca)}}/[\mathrm{Ca}^{2+}]_{\mathrm{cyto}})^3} \tag{59}$$

$$\bar{I}_{\mathrm{ns(K)}} = P_{\mathrm{ns(K)}} \frac{VF^2}{RT} \frac{0.75([\mathrm{K}^+]\mathrm{e}^{VF/RT} - [\mathrm{K}^+]_o)}{\mathrm{e}^{VF/RT} - 1} \tag{60}$$

$$\bar{I}_{\mathrm{ns(Na)}} = P_{\mathrm{ns(Na)}} \frac{VF^2}{RT} \frac{0.75([\mathrm{Na}^+]\mathrm{e}^{VF/RT} - [\mathrm{Na}^+]_o)}{\mathrm{e}^{VF/RT} - 1} \tag{61}$$

$P_{\mathrm{ns(Ca)}}$: Permeability of a channel to Na and K (cm/s)
$K_{\mathrm{m,ns(Ca)}}$: Half-saturation concentration of NSCa channel (mM)
$\bar{I}_{\mathrm{ns(K)}}$: Maximum K current through NSCa channel (μA/μF)
$\bar{I}_{\mathrm{ns(Na)}}$: Maximum Na current through NSCa channel (μA/μF)
P_{Na} : Permeability of the membrane to Na (cm/s)

Sarcolemmal Ca^{2+} pump current

$$I_{\mathrm{pCa}} = I_{\mathrm{pCa}}^{\max} f_{\mathrm{pCa}}^{\mathrm{ATP}} \frac{[\mathrm{Ca}^{2+}]_{\mathrm{cyto}}}{K_m^{\mathrm{pCa}} + [\mathrm{Ca}^{2+}]_{\mathrm{cyto}}} \tag{62}$$

$$f_{\mathrm{pCa}}^{\mathrm{ATP}} = \left(1 + \frac{K_{\mathrm{m1pCa}}^{\mathrm{ATP}}}{[\mathrm{ATP}]_{\mathrm{cyto}}} \left(1 + \frac{[\mathrm{ADP}]_{\mathrm{cyto}}}{K_{\mathrm{i,pCa}}^{\mathrm{ADP}}}\right)\right)^{-1} + \left(1 + \frac{K_{\mathrm{m1pCa}}^{\mathrm{ATP}}}{[\mathrm{ATP}]_{\mathrm{cyto}}}\right)^{-1} \tag{63}$$

$I_{\mathrm{pCa}}^{\max}$: Max.Ca current through the sarcolemmal Ca pump (μA/μF)
K_m^{pCa} : Half-saturation concentration of the sarcolemmal Ca pump
$f_{\mathrm{pCa}}^{\mathrm{ATP}}$: ATP ADP dependence of the sarcolemmal Ca pump

Ca^{2+} background current

$$I_{\mathrm{Ca,b}} = \bar{G}_{\mathrm{Ca,b}} \cdot (V - E_{\mathrm{Ca,N}}) \tag{64}$$

$$E_{\mathrm{Ca,N}} = \frac{RT}{2F} \ln\left(\frac{[\mathrm{Ca}^{2+}]_o}{[\mathrm{Ca}^{2+}]_{\mathrm{cyto}}}\right) \tag{65}$$

$\bar{G}_{\mathrm{Ca,b}}$: Maximum conductance of Ca background (mS/μF)
$E_{\mathrm{Ca,N}}$: Nernst potential for Ca^{2+} (mV)

Na background current

$$I_{\mathrm{Na,b}} = \bar{G}_{\mathrm{Na,b}} \cdot (V - E_{\mathrm{Na,N}}) \tag{66}$$

$$E_{\mathrm{Na,N}} = E_{\mathrm{Na}} = \frac{RT}{F} \ln \left(\frac{[\mathrm{Na}^+]_o}{[\mathrm{Na}^+]} \right) \tag{67}$$

$\bar{G}_{\mathrm{Na,b}}$: Maximum conductance of Na background (mS/μF)
$E_{\mathrm{Na,N}}$: Nernst potential for Na (mV)

L-type Ca^{2+} channel current LCCs locate in the sub-space and surface sarcolemma, therefore regional Ca^{2+} transients have variation.We need to use different models depending on the particular regions in the myocyte because the currently proposed models are created and tuned phenomenologically to either of the regional transients.

L-type Ca^{2+} channel current at the Ca^{2+} release site L-type Ca^{2+} channel currents at the Ca^{2+} release site node are adopted from Cortassa et al. [5] and expressed as follows:

$$I_{\mathrm{Ca_{max}}} = 4\bar{P}_{\mathrm{Ca}}^{\mathrm{CaRU}} \frac{VF^2}{RT} \frac{0.001\mathrm{e}^{2VF/RT} - 0.341[\mathrm{Ca}^{2+}]_o}{\mathrm{e}^{2VF/RT} - 1} \tag{68}$$

$$I_{\mathrm{Ca}} = 6I_{\mathrm{Ca_{max}}} y \cdot O \tag{69}$$

$$I_{\mathrm{K}} = P'_K y \cdot (O + O_{\mathrm{Ca}}) \frac{VF^2}{RT} \frac{[\mathrm{K}^+]\mathrm{e}^{2VF/RT} - [\mathrm{K}^+]_o}{\mathrm{e}^{VF/RT} - 1} \tag{70}$$

$$P'_K = \frac{\bar{P}_K^{\mathrm{CaRU}}}{1 + \frac{I_{\mathrm{Ca_{max}}}}{I_{\mathrm{Ca_{half}}}}}. \tag{71}$$

The LCC state is expressed with the following 13 modes, and the open probability is expressed as $y \cdot (O + O_{\mathrm{Ca}})$ as described above.

$$\frac{dC_0}{dt} = \beta C_1 + \omega C_{\mathrm{Ca0}} - (4\alpha + \gamma) C_0 \tag{72}$$

$$\frac{dC_1}{dt} = 4\alpha C_0 + 2\beta C_2 + \frac{\omega}{b} C_{\mathrm{Ca1}} - (\beta + 3\alpha + \gamma a) C_1 \tag{73}$$

$$\frac{dC_2}{dt} = 3\alpha C_1 + 3\beta C_3 + \frac{\omega}{b^2} C_{\mathrm{Ca2}} - (2\beta + 2\alpha + \gamma a^2) C_2 \tag{74}$$

$$\frac{dC_3}{dt} = 2\alpha C_2 + 4\beta C_4 + \frac{\omega}{b^3} C_{\mathrm{Ca3}} - (3\beta + \alpha + \gamma a^3) C_3 \tag{75}$$

$$\frac{dC_4}{dt} = \alpha C_3 + gO + \frac{\omega}{b^4} C_{\mathrm{Ca4}} - (4\beta + f + \gamma a^4) C_4 \tag{76}$$

$$\frac{dO}{dt} = fC_4 - gO \tag{77}$$

$$\frac{dC_{\mathrm{Ca0}}}{dt} = \beta' C_{\mathrm{Ca1}} + \gamma C_0 - (4\alpha' + \omega) C_{\mathrm{Ca0}} \tag{78}$$

$$\frac{dC_{\mathrm{Ca1}}}{dt} = 4\alpha' C_{\mathrm{Ca0}} + 2\beta' C_{\mathrm{Ca2}} + \gamma a C_1 - (\beta' + 3\alpha' + \frac{\omega}{b}) C_{\mathrm{Ca1}} \tag{79}$$

$$\frac{dC_{\mathrm{Ca2}}}{dt} = 3\alpha' C_{\mathrm{Ca1}} + 3\beta' C_{\mathrm{Ca3}} + \gamma a^2 C_2 - (2\beta' + 2\alpha' + \frac{\omega}{b^2}) C_{\mathrm{Ca2}} \tag{80}$$

$$\frac{dC_{\mathrm{Ca3}}}{dt} = 2\alpha' C_{\mathrm{Ca2}} + 4\beta' C_{\mathrm{Ca4}} + \gamma a^3 C_3 - (3\beta' + \alpha' + \frac{\omega}{b^3}) C_{\mathrm{Ca3}} \tag{81}$$

$$\frac{dC_{\mathrm{Ca4}}}{dt} = \alpha' C_{\mathrm{Ca3}} + g' O_{\mathrm{Ca}} + \gamma a^4 C_4 - (4\beta' + f + \frac{\omega}{b^4}) C_{\mathrm{Ca4}} \tag{82}$$

$$\frac{dO_{\mathrm{Ca}}}{dt} = f' C_{\mathrm{Ca4}} - g' O_{\mathrm{Ca}} \tag{83}$$

$$\frac{dy}{dt} = \frac{y_\infty - y}{\tau_y} \tag{84}$$

where,

$$\alpha = 0.4\mathrm{e}^{(V+12)/10} \tag{85}$$

$$\beta = 0.05\mathrm{e}^{(V+12)/13} \tag{86}$$

$$\alpha' = a\alpha \tag{87}$$

$$\beta' = \frac{\beta}{b} \tag{88}$$

$$\gamma = 0.1875[\mathrm{Ca}^{2+}]_{\mathrm{SS}} \tag{89}$$

$$y_\infty = \frac{1}{1+\mathrm{e}^{((V+55)/7.5)}} + \frac{0.5}{1+\mathrm{e}^{((-V+21)/6)}} \tag{90}$$

$$\tau_y = 20 + \frac{600}{1+e((V+30)/9.5)}. \tag{91}$$

L-type Ca^{2+} channel current except at the Ca^{2+} release site We used model by Luo and Rudy (1995)[26] for the small fraction of LCC outside the release site.

$$I_{\mathrm{Ca}} = 4\bar{P}_{\mathrm{Ca}} d \cdot f \cdot f_{\mathrm{Ca}} \frac{VF^2}{RT} \frac{0.001\mathrm{e}^{2VF/RT} - 0.341[\mathrm{Ca}^{2+}]_o}{\mathrm{e}^{2VF/RT} - 1} \tag{92}$$

where

$$d_\infty = \frac{1}{1+\mathrm{e}^{-(10+V)/6.24}} \tag{93}$$

$$\tau_d = d_\infty \frac{1-\mathrm{e}^{-(10+V)/6.24}}{0.035(10+V)} \tag{94}$$

$$\alpha_d = \frac{d_\infty}{\tau_d} \tag{95}$$

$$\beta_d = \frac{1-\alpha_d}{\tau_d} \tag{96}$$

$$f_\infty = \frac{1}{1+\mathrm{e}^{(V+32)/8}} + \frac{0.6}{1+\mathrm{e}^{(50-V)/20}} \tag{97}$$

$$\tau_f = \frac{1}{0.0197\mathrm{e}^{-[0.0337(V+10)]^2} + 0.02} \tag{98}$$

$$\alpha_f = \frac{f_\infty}{\tau_f} \tag{99}$$

$$\beta_f = \frac{1-\alpha_f}{\tau_f} \tag{100}$$

$$f_{\mathrm{Ca}} = \frac{1}{(1+[\mathrm{Ca}^{2+}]_{\mathrm{cyto}}/K_{m,Ca}} \tag{101}$$

Table S 5: Channel fractions on the surface membrane and t-tubule membrane

Ion current	parameter	total	surface	t-tubule	unit	fraction(t)
I_{Na}	$\bar{G}_{\mathrm{Na}}$	12.8	14.7	11.0	mS/μF	0.57
I_{Kp}	$\bar{G}_{\mathrm{Kp}}$	8.28 $\times 10^{-3}$	-	-	mS/μF	0.50
I_{K1}	$\bar{G}_{\mathrm{K1}}$	0.75	0.3	1.2	mS/μF	0.80
I_{NaK}	$\bar{I}_{\mathrm{NaK}}$	3.147	-	-	μA/μF	0.50
$I_{\mathrm{ns(Na)}}$	$P_{\mathrm{ns(Na)}}$	1.75 $\times 10^{-7}$	-	-	cm/s	0.50
I_{Cab}	G_{Cab}	3.217 $\times 10^{-3}$	-	-	mS/μF	0.50
I_{Nab}	G_{Nab}	5.45 $\times 10^{-4}$	-	-	mS/μF	0.50
I_{pCa}	$I_{\mathrm{pCa}}^{\mathrm{max}}$	0.575	0.828	0.207	μA/μF	0.20
I_{Ca}	$\bar{P}_{\mathrm{Ca}}$	0.916 10^{-3}	16.725 10^{-3}	0.0836 10^{-3}	cm/s	0.91
I_{Na}	$\bar{P}_{\mathrm{K}}$	1.11 $\times 10^{-11}$	-	-	cm/s	0.50

Table S 6: Surface membrane and t-tubule membrane common parameters

parameter	value	unit	reference
C_{mbr}	1.0	μF/cm^2	[5]
$[\mathrm{Na}^+]_o$	140.0	mM	[5]
$[\mathrm{K}^+]_o$	5.4	mM	[5]
$[\mathrm{Ca}^{2+}]_o$	2.0	mM	[5]
P_{NaK}	0.01833		[5]
k_{NaCa}	3000	μA/μF	[5],[26]*
k_{mNa}	87.5	mM	[5]
k_{mCa}	1.38	mM	[5]
k_{sat}	0.1		[5]
η	0.35		[5]
K_{mNai}	10.0	mM	[5]
K_{mKo}	1.5	mM	[5]
$P_{\mathrm{ns(K)}}$	0.00	cm/s	[5]
G_{Cab}	3.217 $\times 10^{-3}$	mS/μF	[5]
G_{Nab}	5.45 $\times 10^{-4}$	mS/μF	[5]
$I_{\mathrm{pCa}}^{\mathrm{max}}$	0.575	μA/μF	[5]

parameter	value	unit	reference
K_m^{pCa}	5.0 $\times 10^{-4}$	mM	[5]
$I_{\mathrm{Ca_{half}}}$	-0.4583	μA/μF	[5]
ω	0.01	ms^{-1}	[5]
a	2.0		[5]
b	2.0		[5]
f	0.3	ms^{-1}	[5]
g	2.0	ms^{-1}	[5]
f'	0.0	ms^{-1}	[5]
g'	0.0	ms^{-1}	[5]
$K_{m,Ca}$	0.0006	mM	[26]

* Na^+-Ca^{2+} exchanger maximum velocity was reduced because the high concentration at the subsarcolemmal space enhanced Na^+-Ca^{2+} flux.

4.4 SR

The reaction term at the JSR node f_{JSR} is:

$$f_{\mathrm{JSR}}(Ca) = J_{\mathrm{xfer}} \tag{102}$$

The JSR Ca^{2+} release site and LCC face each other across the subspace. The JSR, LCC and SS share the same node in our model. Inside the SS and JSR, Ca^{2+} concentrations are defined and change as follows:

$$\frac{\mathrm{d}[\mathrm{Ca}^{2+}]_{\mathrm{SS}}}{\mathrm{d}t} = J_{\mathrm{rel}}\frac{\mathrm{vol}_{\mathrm{JSR}}}{\mathrm{vol}_{\mathrm{SS}}} - J_{\mathrm{xfer}}\frac{\mathrm{vol}_{\mathrm{cyto}}}{\mathrm{vol}_{\mathrm{SS}}} + I_{\mathrm{LCC}}\frac{\mathrm{area}}{2\mathrm{vol}_{\mathrm{SS}}F} \tag{103}$$

$$\frac{\mathrm{d}[\mathrm{Ca}^{2+}]_{\mathrm{JSR}}}{\mathrm{d}t} = \left(1 + \frac{K_{\mathrm{CMDN}}^{\mathrm{SS}}[\mathrm{CMDN}]_{\mathrm{tot}}^{\mathrm{SS}}}{(K_{\mathrm{CMDN}}^{\mathrm{SS}} + [\mathrm{Ca}^{2+}]_{\mathrm{SS}})^2}\right)^{-1}(J_{\mathrm{tr}} - J_{\mathrm{rel}}) \tag{104}$$

The reaction terms at the NSR node f_{NSR} become:

$$f_{\mathrm{NSR}}^{\mathrm{Ca}^{2+}} = -J_{\mathrm{up}}\frac{\mathrm{vol}_{\mathrm{NSR}}}{\mathrm{vol}_{\mathrm{cyto}}} \tag{105}$$

$$f_{\mathrm{NSR}}^{\mathrm{ADP}} = +0.5J_{\mathrm{up}}\frac{\mathrm{vol}_{\mathrm{NSR}}}{\mathrm{vol}_{\mathrm{cyto}}} \tag{106}$$

$$f_{\mathrm{NSR}}^{\mathrm{ATP}} = -0.5J_{\mathrm{up}}\frac{\mathrm{vol}_{\mathrm{NSR}}}{\mathrm{vol}_{\mathrm{cyto}}} \tag{107}$$

Ca^{2+} concentrations inside the NSR are also defined and change as follows:

$$\frac{\mathrm{d}[\mathrm{Ca}^{2+}]_{\mathrm{NSR}}}{\mathrm{d}t} = J_{\mathrm{up}} - J_{\mathrm{tr}}\frac{\mathrm{vol}_{\mathrm{JSR}}}{\mathrm{vol}_{\mathrm{NSR}}} \tag{108}$$

Since J_{xfer} is defined as the change in rate of JSR Ca^{2+} concentration, A correction was made by multiplying by the volume ratio between the SS and the cytosol. On the other hand, J_{up} of the NSR was defined based on cytosolic Ca^{2+} concentration, and no correction was made.

SERCA pump The pumping function of SERCA is dependent on energy metabolite concentration.

$$J_{\mathrm{up}} = K_{\mathrm{SR}} \frac{V_f^{\max} f_b - V_r^{\max} r_b}{1 + f_b + r_b} f_{\mathrm{SERCA}}^{\mathrm{ATP}} \tag{109}$$

$$f_b = \left(\frac{[\mathrm{Ca}^{2+}]_{\mathrm{cyto}}}{K_{fb}} \right)^{\mathrm{N_{fb}}} \tag{110}$$

$$r_b = \left(\frac{[\mathrm{Ca}^{2+}]_{\mathrm{NSR}}}{K_{rb}} \right)^{\mathrm{N_{rb}}} \tag{111}$$

$$f_{\mathrm{SERCA}}^{\mathrm{ATP}} = \left(\frac{K_{\mathrm{m,up}}^{\mathrm{ATP}}}{[\mathrm{ATP}]_{\mathrm{cyto}}} \left(1 + \frac{[\mathrm{ADP}]_{\mathrm{cyto}}}{K_{\mathrm{i,up}}} \right) + \left[1 + \frac{[\mathrm{ADP}]_{\mathrm{cyto}}}{K'_{\mathrm{i,up}}} \right] \right)^{-1} \tag{112}$$

ν_3 : Maximum velocity of Ca^{2+} pumping by SERCA

Ca^{2+} release from the JSR to the SS

$$J_{\mathrm{rel}} = \nu_1 \cdot (RyRopen)([\mathrm{Ca}^{2+}]_{\mathrm{JSR}} - [\mathrm{Ca}^{2+}]_{\mathrm{SS}}) \tag{113}$$

$$RyRopen = v_{\max} \mathrm{e}^{-0.07(t-t_0)} \left(1 - \mathrm{e}^{-0.07(t-t_0)} \right) \tag{114}$$

ν_1 : Maximum Ca^{2+} flux *RyRopen* : RyR open probability t_0 : The time when Ca^{2+} exceeds the threshold

Transport from the NSR to the JSR

$$J_{\mathrm{tr}} = \frac{[\mathrm{Ca}^{2+}]_{\mathrm{NSR}} - [\mathrm{Ca}^{2+}]_{\mathrm{JSR}}}{\tau_{\mathrm{tr}}}, \tag{115}$$

τ_{tr} : Time constant of Ca^{2+} transfer from the NSR to the JSR

Diffusion from the SS to the cytosolic space

$$J_{\mathrm{xfer}} = \frac{[\mathrm{Ca}^{2+}]_{\mathrm{SS}} - [\mathrm{Ca}^{2+}]_{\mathrm{cyto}}}{\tau_{\mathrm{xfer}}}, \tag{116}$$

τ_{xfer} : Time constant of Ca^{2+} from the SS to the cytosol

Table S 7: SR model constants

parameter	value	unit	ref.
$V_f^{\max}$	5.5172 $\times 10^{-3}$	mmol L(NSR)$^{-1}$ ms^{-1}	[5]*
$V_r^{\max}$	5.8681 $\times 10^{-3}$	mmol L(NSR)$^{-1}$ ms^{-1}	[5]*
K_{fb}	2.4 $\times 10^{-4}$	mM	[5]
K_{rb}	1.64269	mM	[5]
N_{fb}	1.787		[27]
N_{rb}	1.0		[5]
$K_{\mathrm{m,up}}^{\mathrm{ATP}}$	0.01	mM	[5]

parameter	value	unit	ref.
$K_{\mathrm{i,up}}$	0.14	mM	[5]
$K'_{\mathrm{i,up}}$	5.1	mM	[5]
ν_1	3.6	ms^{-1}	[5]
τ_{xfer}	0.1	ms	[5]**
τ_{tr}	0.574713	ms	[5]
K_{CSQN}	0.8	mM	[5]
$[\mathrm{CSQN}]_{\mathrm{tot}}$	15.0	mM	[5]
$K^{\mathrm{SS}}_{\mathrm{CMDN}}$	2.38×10^{-3}	mM	[5]
$[\mathrm{CMDN}]^{\mathrm{SS}}_{\mathrm{tot}}$	5.0×10^{-2}	mM	[5]

* $V_f^{\max}$ and $V_r^{\max}$ are converted from mmol [L(cyto)$^{-1}$ ms^{-1}] to [mmol L(NSR)$^{-1}$ ms^{-1}].

** In the original model by Cortassa et al., [5] τ_{xfer} denotes a time constant for Ca^{2+} diffusion from the SS to the bulk cytosolic space. In our model, however, τ_{xfer} is the time constant for the diffusion from the SS to the adjacent cytosolic node. This definition inherently meant that the τ_{xfer} value was dependent on the mesh size. Accordingly, we set the τ_{xfer} value at 0.1 so that the average cytosolic Ca^{2+} transient reproduced physiological levels.

4.5 Mitochondria

Reaction terms at the mitochondrial node f_{mito} are described as follows:

$$f^{\mathrm{Ca}^{2+}}_{\mathrm{mito}} = -(V_{\mathrm{uni}} - V_{\mathrm{NaCa}})\frac{\mathrm{vol}_{\mathrm{mito}}}{\mathrm{vol}_{\mathrm{cyto}}} \tag{117}$$

$$f^{\mathrm{ADP}}_{\mathrm{mito}} = -V_{\mathrm{ANT}}\frac{\mathrm{vol}_{\mathrm{mito}}}{\mathrm{vol}_{\mathrm{cyto}}} \tag{118}$$

$$f^{\mathrm{ATP}}_{\mathrm{mito}} = +V_{\mathrm{ANT}}\frac{\mathrm{vol}_{\mathrm{mito}}}{\mathrm{vol}_{\mathrm{cyto}}} \tag{119}$$

At each node in mitochondria, ten variables are additionaly defined:

$[\mathrm{ADP}]_m$: Mitochondrial ADP concentration.

[NADH]: Mitochondrial NADH concentration.

[ISOC]: Mitochondrial isocitrate concentration.

[aKG] : Mitochondrial α-ketoglutarate concentration.

[SCoA]: Mitochondrial succinyl CoA concentration.

[Suc] : Mitochondrial succinate concentration.

[FUM] : Mitochondrial fumarate concentration.

[MAL] : Mitochondrial malate concentration.

[OAA] : Mitochondrial oxalacetate concentration.

$[\mathrm{Ca}]_m$: Mitochondrial free Ca^{2+} concentration.

$\Delta\Psi_m$: Inner mitochondrial membrane potential (This variable takes the common value at all nodes in a single mitochondria.)

Reaction term eqns.(117,118,119) were determined in terms of the cytosolic substrate concentration and the above 11 variables.

Time derivatives of the 11 variables are described as follows:

$$\frac{d[\mathrm{ADP}]_{\mathrm{mito}}}{dt} = V_{\mathrm{ANT}} - V_{\mathrm{ATPase}} - V_{\mathrm{SL}} \tag{120}$$

$$\frac{d[\mathrm{NADH}]}{dt} = -V_{\mathrm{O2}} + V_{\mathrm{IDH}} + V_{\mathrm{KGDH}} + V_{\mathrm{MDH}} \tag{121}$$

$$\frac{d[\mathrm{ISOC}]}{dt} = V_{\mathrm{ACO}} - V_{\mathrm{IDH}} \tag{122}$$

$$\frac{d[\mathrm{aKG}]}{dt} = V_{\mathrm{IDH}} - V_{\mathrm{KGDH}} + V_{\mathrm{AAT}} \tag{123}$$

$$\frac{d[\mathrm{SCoA}]}{dt} = V_{\mathrm{KGDH}} - V_{\mathrm{SL}} \tag{124}$$

$$\frac{d[\mathrm{Suc}]}{dt} = V_{\mathrm{SL}} - V_{\mathrm{SDH}} \tag{125}$$

$$\frac{d[\mathrm{FUM}]}{dt} = V_{\mathrm{SDH}} - V_{\mathrm{FH}} \tag{126}$$

$$\frac{d[\mathrm{MAL}]}{dt} = V_{\mathrm{FH}} - V_{\mathrm{MDH}} \tag{127}$$

$$\frac{d[\mathrm{OAA}]}{dt} = V_{\mathrm{MDH}} - V_{\mathrm{CS}} - V_{\mathrm{AAT}} \tag{128}$$

$$\frac{d[\mathrm{Ca}^{2+}]_{\mathrm{mito}}}{dt} = \beta_{\mathrm{mitCa}}(V_{\mathrm{uni}} - V_{\mathrm{NaCa}}) \tag{129}$$

$$\frac{d\Delta\Psi_{\mathrm{mito}}}{dt} = \frac{1}{C_{\mathrm{mito}}} \sum_{\mathrm{mitochondrion}} (V_{\mathrm{He}} + V_{\mathrm{HeF}} - V_{\mathrm{Hu}} - V_{\mathrm{ANT}} + V_{\mathrm{Hleak}} - V_{\mathrm{NaCa}} - 2V_{\mathrm{uni}}) \tag{130}$$

$V_\circ$ denotes the reaction velocities [mmolL^{-1}ms^{-1}] of $\circ$ proteins, which are listed in the following sections. β_{mitCa} is the fraction of free Ca^{2+}, analogous to cytosolic Ca^{2+} buffer as follows:

$$\beta_{\mathrm{mitCa}} = \left(1 + \frac{K_{\mathrm{Buf}}[\mathrm{Buf}]_{\mathrm{tot}}}{(K_{\mathrm{Buf}} + [\mathrm{Ca}^{2+}]_{\mathrm{mito}})^2}\right)^{-1} \tag{131}$$

where $[\mathrm{Buf}]_{\mathrm{tot}}$ is the concentration of Ca^{2+} buffer in mitochondria and K_{Buf} is the Ca^{2+} half saturation constant for Ca^{2+} buffer. $[\mathrm{Buf}]_{\mathrm{tot}}$, K_{Buf}, and even the buffer itself are unknown. Because the fraction of free Ca^{2+} is estimated to be approximately 1% [30], we set the values so that β_{mitCa} becomes 0.01 when $[\mathrm{Ca}^{2+}]_{\mathrm{mito}}$ is 0.1 μmol/L.

The following are dependent variables:

$$[\mathrm{NAD}] = C_{\mathrm{PN}} - [\mathrm{NADH}] \tag{132}$$

$$[\mathrm{ATP}]_{\mathrm{mito}} = C_m - [\mathrm{ADP}]_{\mathrm{mito}} \tag{133}$$

$$[\mathrm{CIT}] = C_{\mathrm{Kint}} - [\mathrm{ISOC}] - [\mathrm{aKG}] - [\mathrm{SCoA}] - [\mathrm{Suc}] - [\mathrm{FUM}] - [\mathrm{MAL}] - [\mathrm{OAA}] \tag{134}$$

4.5.1 TCA cycle model

Cytrate synthase

$$V_{\mathrm{CS}} = k_{\mathrm{cat}}^{\mathrm{CS}} E_{\mathrm{T}}^{\mathrm{CS}} \left(1 + \frac{K_{\mathrm{M}}^{\mathrm{AcCoA}}}{[\mathrm{AcCoA}]} + \frac{K_{\mathrm{M}}^{\mathrm{OAA}}}{[\mathrm{OAA}]} + \frac{K_{\mathrm{M}}^{\mathrm{AcCoA}}}{[\mathrm{AcCoA}]} \frac{K_{\mathrm{M}}^{\mathrm{OAA}}}{[\mathrm{OAA}]}\right)^{-1} \tag{135}$$

Aconitase

$$V_{\mathrm{ACO}} = k_f^{\mathrm{ACO}} \left([\mathrm{CIT}] - \frac{[\mathrm{ISOC}]}{K_E^{\mathrm{ACO}}}\right) \tag{136}$$

Isocitrate dehydrogenase

$$V_{\mathrm{IDH}} = \frac{k_{\mathrm{cat}}^{\mathrm{IDH}} E_{\mathrm{T}}^{\mathrm{IDH}}}{\left(1 + \frac{[\mathrm{H}^+]}{k_{\mathrm{h},1}} + \frac{k_{\mathrm{h},2}}{[\mathrm{H}^+]} + f_i^{\mathrm{IDH}} \left(\frac{K_{\mathrm{M,IDH}}^{\mathrm{NAD}}}{[\mathrm{NAD}]}\right) + f_a^{\mathrm{IDH}} \left(\frac{K_{\mathrm{M}}^{\mathrm{ISOC}}}{[\mathrm{ISOC}]}\right)^{n_{\mathrm{i}}} + f_a^{\mathrm{IDH}} f_i^{\mathrm{IDH}} \left(\frac{K_{\mathrm{M}}^{\mathrm{ISOC}}}{[\mathrm{ISOC}]}\right)^{n_{\mathrm{i}}} \left(\frac{K_{\mathrm{M,IDH}}^{\mathrm{NAD}}}{[\mathrm{NAD}]}\right)\right)}$$

$$f_a^{\mathrm{IDH}} = \left[\left(1 + \frac{[\mathrm{ADP}]_{\mathrm{mito}}}{K_{\mathrm{ADP}}^a}\right)\left(1 + \frac{[\mathrm{Ca}^{2+}]_{\mathrm{mito}}}{K_{\mathrm{Ca}}^a}\right)\right]^{-1} \tag{137}$$

$$f_i^{\mathrm{IDH}} = \left(1 + \frac{[\mathrm{NADH}]}{K_{\mathrm{i,NADH}}}\right) \tag{138}$$

Alpha-ketoglutarate dehydrogenase

$$V_{\mathrm{KGDH}} = \frac{k_{\mathrm{cat}}^{\mathrm{KGDH}} E_{\mathrm{T}}^{\mathrm{KGDH}}}{1 + f_a^{\mathrm{KGDH}} \left(\frac{K_{\mathrm{M}}^{\alpha\mathrm{KG}}}{[\alpha\mathrm{KG}]}\right)^{n_{\alpha\mathrm{KG}}} + f_a^{\mathrm{KGDH}} \frac{K_{\mathrm{M,KG}}^{\mathrm{NAD}}}{[\mathrm{NAD}]}} \tag{139}$$

$$f_a^{\mathrm{KGDH}} = \left[\left(1 + \frac{[\mathrm{Mg}^{2+}]}{K_{\mathrm{D}}^{\mathrm{Mg}^{2+}}}\right)\left(1 + \frac{[\mathrm{Ca}^{2+}]}{K_{\mathrm{D}}^{\mathrm{Ca}^{2+}}}\right)\right]^{-1} \tag{140}$$

Succinyl lyase

$$V_{\mathrm{SL}} = k_f^{\mathrm{SL}} \left([\mathrm{SCoA}][\mathrm{ADP}]_{\mathrm{mito}} - \frac{[\mathrm{Suc}][\mathrm{ATP}]_{\mathrm{mito}}[\mathrm{CoA}]}{K_E^{\mathrm{SL}}}\right) \tag{141}$$

Succinate dehydrogenase

$$V_{\mathrm{SDH}} = \frac{k_{\mathrm{cat}}^{\mathrm{SDH}} E_{\mathrm{T}}^{\mathrm{SDH}}}{1 + \left(\frac{K_{\mathrm{M}}^{\mathrm{Suc}}}{[\mathrm{Suc}]}\right)\left(1 + \frac{[\mathrm{OAA}]}{K_{\mathrm{i,SDH}}^{\mathrm{OAA}}}\right)\left(1 + \frac{[\mathrm{FUM}]}{K_{\mathrm{i}}^{\mathrm{FUM}}}\right)} \tag{142}$$

Fumarate hydratase

$$V_{\mathrm{FH}} = k_f^{\mathrm{FH}} \left([\mathrm{FUM}] - \frac{[\mathrm{MAL}]}{K_E^{\mathrm{FH}}}\right) \tag{143}$$

Malate dehydrogenase

$$V_{\mathrm{MDH}} = \frac{k_{\mathrm{cat}}^{\mathrm{MDH}} E_{\mathrm{T}}^{\mathrm{MDH}} f_{\mathrm{h,a}} f_{\mathrm{h,i}}}{1 + \left(\frac{K_{\mathrm{M}}^{\mathrm{MAL}}}{[\mathrm{MAL}]}\right)\left(1 + \frac{[\mathrm{OAA}]}{K_i^{\mathrm{OAA}}}\right) + \left(\frac{K_{\mathrm{M,MDH}}^{\mathrm{NAD}}}{[\mathrm{NAD}]}\right) + \left(\frac{K_{\mathrm{M}}^{\mathrm{MAL}}}{[\mathrm{MAL}]}\right)\left(1 + \frac{[\mathrm{OAA}]}{K_i^{\mathrm{OAA}}}\right)\left(\frac{K_{\mathrm{M,MDH}}^{\mathrm{NAD}}}{[\mathrm{NAD}]}\right)} \tag{144}$$

$$f_{\mathrm{h,a}} = \left(1 + \frac{[\mathrm{H}^+]}{k_{\mathrm{h},1}} + \frac{[\mathrm{H}^+]^2}{k_{\mathrm{h},1} k_{\mathrm{h},2}}\right)^{-1} + k_{\mathrm{offset}} \tag{145}$$

$$f_{\mathrm{h,i}} = \left(1 + \frac{k_{\mathrm{h},3}}{[\mathrm{H}^+]} + \frac{k_{\mathrm{h},3} k_{\mathrm{h},4}}{[\mathrm{H}^+]^2}\right)^{-2} \tag{146}$$

Aspartate amino trasferase

$$V_{\mathrm{AAT}} = k_f^{\mathrm{AAT}} [\mathrm{OAA}][\mathrm{GLU}] \frac{k_{\mathrm{ASP}} K_E^{\mathrm{AAT}}}{k_{\mathrm{ASP}} K_E^{\mathrm{AAT}} + [\alpha\mathrm{KG}] k_f^{\mathrm{AAT}}} \tag{147}$$

4.5.2 Oxidative phophorylation

Proton motive force

$$\Delta\mu_{\mathrm{H}} = -2.303 \frac{RT}{F} \Delta pH + \Delta\Psi_{\mathrm{m}} \tag{148}$$

Oxygen consumption

$$V_{\mathrm{O2}} = 0.5 \rho^{\mathrm{res}} \frac{\left(r_a + r_{c1} \mathrm{e}^{\frac{6F\Delta\Psi_B}{RT}}\right) \mathrm{e}^{\frac{A_{\mathrm{res}} F}{RT}} - r_a \mathrm{e}^{\frac{g6F\Delta\mu_H}{RT}} + r_{c2} \mathrm{e}^{\frac{A_{\mathrm{res}} F}{RT}} \mathrm{e}^{\frac{g6F\Delta\mu_H}{RT}}}{(1 + r_1 \mathrm{e}^{\frac{A_{\mathrm{res}} F}{RT}}) \mathrm{e}^{\frac{6F\Delta\Psi_B}{RT}} + (r_2 + r_3 \mathrm{e}^{\frac{A_{\mathrm{res}} F}{RT}}) \mathrm{e}^{\frac{g6F\Delta\mu_H}{RT}}} \tag{149}$$

Proton pumping of complexes I-IV

$$V_{\mathrm{He}} = 6 \rho^{\mathrm{res}} \frac{r_a \mathrm{e}^{\frac{A_{\mathrm{res}} F}{RT}} - (r_a + r_b) \mathrm{e}^{\frac{g6F\Delta\mu_H}{RT}}}{(1 + r_1 \mathrm{e}^{\frac{A_{\mathrm{res}} F}{RT}}) \mathrm{e}^{\frac{6F\Delta\Psi_B}{RT}} + (r_2 + r_3 \mathrm{e}^{\frac{A_{\mathrm{res}} F}{RT}}) \mathrm{e}^{\frac{g6F\Delta\mu_H}{RT}}} \tag{150}$$

$$A_{\mathrm{res}} = \frac{RT}{F} \ln\left(K_{\mathrm{res}} \sqrt{\frac{[\mathrm{NADH}]}{[\mathrm{NAD}^+]}}\right) \tag{151}$$

$$V_{\mathrm{He(F)}} = 4 \rho^{\mathrm{res(F))}} \frac{r_a \mathrm{e}^{\frac{A_{\mathrm{res(F)}} F}{RT}} - (r_a + r_b) \mathrm{e}^{\frac{g6F\Delta\mu_H}{RT}}}{(1 + r_1 \mathrm{e}^{\frac{A_{\mathrm{res(F)}} F}{RT}}) \mathrm{e}^{\frac{6F\Delta\Psi_B}{RT}} + (r_2 + r_3 \mathrm{e}^{\frac{A_{\mathrm{res(F)}} F}{RT}}) \mathrm{e}^{\frac{g6F\Delta\mu_H}{RT}}} \tag{152}$$

$$A_{\mathrm{res(F)}} = \frac{RT}{F} \ln\left(K_{\mathrm{res(F)}} \sqrt{\frac{[\mathrm{FADH_2}]}{[\mathrm{FAD}]}}\right) \tag{153}$$

ATP synthesis and proton flux

$$V_{\mathrm{ATPase}} = -\rho^{\mathrm{F1}}\frac{(10^2 p_a + p_{c1}\mathrm{e}^{\frac{3F\Delta\Psi_B}{RT}})\mathrm{e}^{\frac{A_{\mathrm{F1}}F}{RT}} - p_a\mathrm{e}^{\frac{3F\Delta\mu_H}{RT}} + p_{c2}\mathrm{e}^{\frac{A_{\mathrm{F1}}}{RT}}\mathrm{e}^{\frac{3F\Delta\mu_H}{RT}}}{(1+p_1\mathrm{e}^{\frac{A_{\mathrm{F1}}F}{RT}})\mathrm{e}^{\frac{3F\Delta\Psi_B}{RT}} + (p_2+p_3\mathrm{e}^{\frac{A_{\mathrm{F1}}F}{RT}})\mathrm{e}^{\frac{3F\Delta\mu_H}{RT}}} \tag{154}$$

$$V_{\mathrm{Hu}} = -3\rho^{\mathrm{F1}}\frac{100p_a\left(1+\mathrm{e}^{\frac{FA_{\mathrm{F1}}}{RT}}\right) - (p_a+p_b)\mathrm{e}^{\frac{3F\Delta\mu_H}{RT}}}{(1+p_1\mathrm{e}^{\frac{A_{\mathrm{F1}}F}{RT}})\mathrm{e}^{\frac{3F\Delta\Psi_B}{RT}} + (p_2+p_3\mathrm{e}^{\frac{A_{\mathrm{F1}}F}{RT}})\mathrm{e}^{\frac{3F\Delta\mu_H}{RT}}} \tag{155}$$

$$A_{\mathrm{F1}} = \frac{RT}{F}\ln\left(K_{\mathrm{F1}}\frac{[\mathrm{ATP}]_{\mathrm{mito}}}{[\mathrm{ADP}]_{\mathrm{mito}}[\mathrm{Pi}]}\right) \tag{156}$$

Adenine nucleotide translocator

$$V_{\mathrm{ANT}} = V_{\mathrm{ANT}}^{\max}\frac{\left(1-\frac{0.05\times[\mathrm{ATP}]_{\mathrm{cyto}}\times0.45\times0.8\times[\mathrm{ADP}]_{\mathrm{mito}}}{0.45\times[\mathrm{ADP}]_{\mathrm{cyto}}\times0.05[\mathrm{ATP}]_{\mathrm{mito}}}\right)}{\left(1+\frac{0.05\times[\mathrm{ATP}]_{\mathrm{cyto}}}{0.45\times[\mathrm{ADP}]_{\mathrm{cyto}}}\mathrm{e}^{\left(-\frac{h_{\mathrm{ANT}}F\Delta\Psi_m}{RT}\right)}\right)\left(1+\frac{0.45\times0.8\times[\mathrm{ADP}]_{\mathrm{mito}}}{0.05\times[\mathrm{ATP}]_{\mathrm{mito}}}\right)} \tag{157}$$

Proton leak

$$V_{\mathrm{Hleak}} = g_{\mathrm{H}}\Delta\mu_{\mathrm{H}} \tag{158}$$

4.5.3 Ca^{2+} handling

Ca^{2+} : mitochondrial Ca^{2+} uniporter

We adopted the model of mitochondrial Ca uniporter kinetics proposed by Dash et al. [31], which is a hybrid model combining the Michaelis-Menten equation for carrier-mediated facilitated transport of Ca^{2+} influx and the Goldman-Hodgkin-Katz equation for electrodiffusion.

$$V_{\mathrm{uni}} = V_{\mathrm{uni}}^{\max}\left(\frac{\Delta\Phi/n_{\mathrm{uni}}}{\sinh(\Delta\Phi/n_{\mathrm{uni}})}\right)^{n_{\mathrm{uni}}}\frac{[\mathrm{Ca}^{2+}]_{\mathrm{cyto}}^2 e^{\Delta\Phi} - [\mathrm{Ca}^{2+}]_{\mathrm{mito}}^2 e^{-\Delta\Phi}}{K_{\mathrm{uni}}^2 + [\mathrm{Ca}^{2+}]_{\mathrm{cyto}}^2 + [\mathrm{Ca}^{2+}]_{\mathrm{mito}}^2} \tag{159}$$

$$\Delta\Phi = \frac{2F\Delta\Psi}{RT} \tag{160}$$

Mitochondrial Na-Ca exchanger

$$V_{\mathrm{NaCa}} = V_{\mathrm{NaCa}}^{\max}\frac{\mathrm{e}^{\frac{b_{\mathrm{NaCa}}F(\Delta\Psi_m-\Delta\Psi^o)}{RT}}\frac{[\mathrm{Ca}^{2+}]_{\mathrm{mito}}}{[\mathrm{Ca}^{2+}]_{\mathrm{cyto}}}}{\left(1+\frac{K_{\mathrm{Na}}}{[\mathrm{Na}^+]}\right)_{\mathrm{NaCa}}^{n}\left(1+\frac{K_{\mathrm{Ca}}}{[\mathrm{Ca}^{2+}]_{\mathrm{cyto}}}\right)} \tag{161}$$

Table S 8: Mitochondrial model parameters

parameter	value	unit	ref.
[AcCoA]	1.0	mM	[5]
[GLU]	10.0	mM	[5]
$k_{\mathrm{cat}}^{\mathrm{CS}}$	0.1	ms^{-1}	[5] *1
$E_{\mathrm{T}}^{\mathrm{CS}}$	0.4	mM	[5]

parameter	value	unit	ref.
$K_{\mathrm{M}}^{\mathrm{AcCoA}}$	1.26×10^{-2}	mM	[5]
$K_{\mathrm{M}}^{\mathrm{OAA}}$	6.4×10^{-4}	mM	[5]
C_{Kint}	1.0	mM	[5]
$k_{\mathrm{f}}^{\mathrm{ACO}}$	1.25×10^{-2}	ms^{-1}	[5]
$K_{\mathrm{E}}^{\mathrm{ACO}}$	2.22	-	[5]
$k_{\mathrm{cat}}^{\mathrm{IDH}}$	0.05	ms^{-1}	[5] *1
$E_{\mathrm{T}}^{\mathrm{IDH}}$	0.109	mM	[5]
n_{i}	2	-	[5]
K_{Ca}^{a}	0.0005	mM	[5]
K_{NADH}^{i}	0.19	mM	[5]
K_{ADP}^{a}	0.062	mM	[5]
$[\mathrm{H}^{+}]$	2.5×10^{-5}	mM	[5]
$k_{\mathrm{h},1}$	8.1×10^{-5}	mM	[5]
$k_{\mathrm{h},2}$	5.98×10^{-5}	mM	[5]
$K_{\mathrm{M}}^{\mathrm{ISOC}}$	1.52	mM	[5]
$K_{\mathrm{M,IDH}}^{\mathrm{NAD}}$	0.923	mM	[5]
$k_{\mathrm{cat}}^{\mathrm{KGDH}}$	0.1	ms^{-1}	[5] *1
$E_{\mathrm{T}}^{\mathrm{KGDH}}$	0.5	mM	[5]
$K_{\mathrm{M}}^{\mathrm{aKG}}$	1.94	mM	[5]
$K_{\mathrm{M,KG}}^{\mathrm{NAD}}$	38.7	mM	[5]
$K_{\mathrm{D}}^{\mathrm{Mg}}$	0.0308	mM	[5]
$K_{\mathrm{D}}^{\mathrm{Ca}}$	1.27×10^{-3}	mM	[5]
n_{aKG}	1.2	-	[5]
$[\mathrm{Mg}^{2+}]$	0.4	mM	[5]
$k_{\mathrm{f}}^{\mathrm{SL}}$	7.5×10^{-3}	$\mathrm{mM}^{-1}\ \mathrm{ms}^{-1}$	[5] *1
$K_{\mathrm{E}}^{\mathrm{SL}}$	3.115	-	[5]
[CoA]	0.02	mM	[5]
$k_{\mathrm{cat}}^{\mathrm{SDH}}$	7.5×10^{-3}	ms^{-1}	[5] *1
$E_{\mathrm{T}}^{\mathrm{SDH}}$	0.5	mM	[5]
$K_{\mathrm{M}}^{\mathrm{Suc}}$	3.0×10^{-2}	mM	[5]
$K_{\mathrm{i}}^{\mathrm{FUM}}$	1.3	mM	[5]
$K_{\mathrm{i,sdh}}^{\mathrm{OAA}}$	0.15	mM	[5]
$k_{\mathrm{f}}^{\mathrm{FH}}$	5.0×10^{-3}	ms^{-1}	[5] *1
$K_{\mathrm{E}}^{\mathrm{FH}}$	1.0	-	[5]

parameter	value	unit	ref.
k_{h1}	1.13×10^{-5}	mM	[5]
k_{h2}	26.7	mM	[5]
k_{h3}	6.68×10^{-9}	mM	[5]
k_{h4}	5.62×10^{-6}	mM	[5]
k_{offset}	3.99×10^{-2}	-	[5]
$k_{\mathrm{cat}}^{\mathrm{MDH}}$	0.1665	ms^{-1}	[5] *1
$E_{\mathrm{T}}^{\mathrm{MDH}}$	0.154	mM	[5]
$K_{\mathrm{M}}^{\mathrm{MAL}}$	1.493	mM	[5]
$K_{\mathrm{i}}^{\mathrm{OAA}}$	3.1×10^{-3}	mM	[5]
$K_{\mathrm{M,MDH}}^{\mathrm{NAD}}$	0.2244	mM	[5]
$k_{\mathrm{f}}^{\mathrm{AAT}}$	9.66×10^{-4}	ms^{-1}	[5] *1
$K_{\mathrm{E}}^{\mathrm{AAT}}$	6.6	-	[5]
k_{ASP}	1.5×10^{-6}	ms^{-1}	[5]
r_a	6.394×10^{-13}	ms^{-1}	[5]
r_b	1.762×10^{-16}	ms^{-1}	[5]
r_{c1}	2.656×10^{-22}	ms^{-1}	[5]
r_{c2}	8.632×10^{-30}	ms^{-1}	[5]
r_1	2.077×10^{-18}	-	[5]
r_2	1.728×10^{-9}	-	[5]
r_3	1.059×10^{-26}	-	[5]
ρ_{res}	0.1	mM	[5] *2
K_{res}	1.35×10^{18}	-	[5]
ρ_{resF}	3.75×10^{-4}	mM	[5]
$\Delta\Psi_{\mathrm{B}}$	50.0	mV	[5]
G	0.85	-	[5]
K_{resF}	5.765×10^{13}	mM	[5]
$[\mathrm{FADH_2}]$	1.24	mM	[5]
[FAD]	0.01	mM	[5]
p_a	1.656×10^{-8}	ms^{-1}	[5]
p_b	3.373×10^{-10}	ms^{-1}	[5]
p_{c1}	9.651×10^{-17}	ms^{-1}	[5]
p_{c2}	4.585×10^{-17}	ms^{-1}	[5]
p_1	1.346×10^{-8}	-	[5]
p_2	7.739×10^{-7}	-	[5]

parameter	value	unit	ref.
p_3	6.65×10^{-15}	-	[5]
ρ_{F1}	0.5	mM	[5] *2
K_{F1}	1.71×10^{6}	-	[5]
C_{A}	1.5	mM	[5]
$V_{\mathrm{ANT}}^{\mathrm{max}}$	1.0	mM ms^{-1}	[5] *2
h_{ANT}	0.5	-	[5]
g_{H}	1.0×10^{-8}	mM ms^{-1} mV^{-1}	[5]
ΔpH	-0.6	pH units	[5]
C_{PN}	10.0	mM	[5]
C_{mito}	1.812×10^{-3}	mM mV^{-1}	[5]
$V_{\mathrm{uni}}^{\mathrm{max}}$	0.5-2.0 $\times10^{-5}$	mM ms^{-1}	[32, 33]*3
n_{uni}	2.7	-	[31]
K_{uni}	10.0×10^{-3}	mM	[31], [33]
n_a	2.8	-	[5]
$V_{\mathrm{NaCa}}^{\mathrm{max}}$	2.0-8.0 $\times10^{-5}$	mM ms^{-1}	[32, 34, 35]*3
b_{NaCa}	0.5	-	[5]
K_{Na}	9.4	mM	[5]
K_{Ca}	3.75×10^{-4}	mM	[5]
n_{NaCa}	3.0	-	[5]
K_{mitCa}	0.002	mM	[5]
[Buf]	1.0	mM	[5]

*1) As have been done in the work by Cortassa et al. [5], the kinetic constants of all the TCA cycle enzyme steps were multiplied by a factor of 2-3 to maintain the physiological level of metabolites against local accumulation of ions and substrates caused by the diffusional barrier.

*2) The constants for oxidative phosphorylation, ρ_{res} and ρ_{F1}, and for the adenine nucleotide translocator $V_{\mathrm{ANT}}^{\mathrm{max}}$ were also adjusted to maintain physiological levels of metabolites against local accumulation of ions and substrates caused by the diffusional barrier..

*3) Mitochondrial Ca^{2+} handling constants ($V_{\mathrm{uni}}^{\mathrm{max}}$ and $V_{\mathrm{NaCa}}^{\mathrm{max}}$) were set so that the averaged value of the spatially heterogenous Ca^{2+} fluxes of the 3D model matched the experimentally obtained fluxes.

References

[1] J. Okada, S. Sugiura, S. Nishimura, and T. Hisada. Three-dimensional simulation of calcium waves and contraction in cardiomyocytes using the finite element method. Am J Physiol, Vol. 288, pp. 510–522, 2005.

[2] S. Subramanian, S. Viatchenko-Karpinski, V. Lukyanenko, S. Gyke, and T. F. Wiesner. Underlying mechanisms of symmetric calcium wave propagation in rat ventricular myocytes. Biophys J, Vol. 80, No. 1, pp. 1–11, 2001.

[3] L. T. Izu, W. G. Wier, and C. W. Balke. Evolution of cardiac calcium waves from stochastic calcium sparks. Biophys J, Vol. 80, No. 1, pp. 103–120, 2001.

[4] G. Lemon. Fire-diffuse-fire calcium waves in confined intracellular spaces. Bulletin of Mathematical Biology, Vol. 66, No. 1, pp. 65–90, 2004.

[5] S. Cortassa, M.A. Aon, B. O'Rourke, R. Jacques, H-J. Tseng, E. Marban, and R.L. Winslow. A computational model integrating electrophysiology, contraction, and mitochondrial bioenergetics in the ventricular myocyte. Biophys J, Vol. 91, pp. 1564–1589, 2006.

[6] Robin A. de Graaf, A. van Kranenburg, and K. Nicolay. In vivo ^{31}P-NMR diffusion spectroscopy of atp and phosphocreatine in rat skeletal muscle. Biophys J, Vol. 78, No. 4, pp. 1657–1664, 2000.

[7] M. Vendelin, M. Lemba, and V.A. Saks. Analysis of functional coupling: Mitochondrial creatine kinase and adenine nucleotide translocase. Biophys J, Vol. 87, pp. 696–713, 2004.

[8] S. Papadopoulos, K. D. Jurgens, and G. Gros. Protein diffusion in living skeletal muscle fibers: Dependence on protein size, fiber type, and contraction. Biophys J, Vol. 79, pp. 2084–2094, 2000.

[9] T. Wallimann, M. Wyss, D. Brdiczka, K. Nicolay, and H.M. Eppenberger. Intracellular compartmentation, structure and function of creatine kinase isoenzymes in tissues with high and fluctuating energy demands: the 'phosphocreatine circuit' for cellular energy homeostasis. Biochem J, Vol. 281, pp. 21–40, 1992.

[10] A. Partikian, B. Olveczky, R. Swaminathan, Y. Li, and A.S. Verkman. Rapid diffusion of green fluorescent protein in the mitochondrial matrix. J Cell Biol, Vol. 140, pp. 4821–4829, 1998.

[11] B. A. Scalettar, J. R. Abney, and C. R. Hackenbrock. Dynamics, structure, and function are coupled in the mitochondrial matrix. Proceedings of the National Academy of Sciences of the United States of America, Vol. 88, No. 18, pp. 8057–8061, 1991.

[12] B. P. Olveczky and A. S. Verkman. Monte carlo analysis of obstructed diffusion in three dimensions: Application to molecular diffusion in organelles. Biophys J., Vol. 74, No. 5, pp. 2722–2730, 1998.

[13] H. Watanabe, S. Sugiura, H. Kafuku, and T. Hisada. Multiphysics simulation of left ventricular filling dynamics using fluid-structure interaction finite element method. Biophys J., Vol. 87, No. 3, pp. 2074–2085, 2004.

[14] J. D. Humphrey, R. K. Strumpf, and F. C. P. Yin. Determination of a constitutive relation for passive myocardium: I. a new functional form. J Biomech Eng, Vol. 112, No. 3, pp. 333–339, 1990.

[15] D. H. S. Lin and F. C. P. Yin. A multiaxial constitutive law for mammalian left ventricular myocardium in steady-state barium contracture or tetanus. Journal of Biomechanical Engineering, Vol. 120, No. 4, pp. 504–517, 1998.

[16] W. A. Linke, V. I. Popov, and G. H. Pollack. Passive and active tension in single cardiac myofibrils. Biophys J, Vol. 67, No. 2, pp. 782–92, 1994.

[17] N. Akiyama, Y. Ohnuki, Y. Kunioka, Y. Saeki, and T. Yamada. Transverse stiffness of myofibrils of skeletal and cardiac muscles studied by atomic force microscopy. J Physiol Sci, Vol. 56, No. 2, pp. 145–51, 2006.

[18] H. E. Smith and E. Page. Morphometry of rat heart mitochondrial subcompartments and membranes: Application to myocardial cell atrophy after hypophysectomy. J Ultra Res, Vol. 55, No. 1, pp. 31–41, 1976.

[19] Y. Chen-Izu, S. L. McCulle, C. W. Ward, C. Soeller, B. M. Allen, C. Rabang, M. B. Cannell, C. W. Balke, and L. T. Izu. Three-dimensional distribution of ryanodine receptor clusters in cardiac myocytes. Biophys J, Vol. 91, No. 1, pp. 1–13, 2006.

[20] D.R.L. Scriven, P. Dan, and E.D.W. Moore. Distribution of poteins implicated in excitation-contraction coupling in rat ventricular myocytes. Biophys J, Vol. 79, pp. 2682–2691, 2000.

[21] C. Soeller and M. B. Cannell. Examination of the transverse tubular system in living cardiac rat myocytes by 2-photon microscopy and digital image processing techniques. Circulation Research, Vol. 84, No. 3, pp. 266–275, 1999. T-tubule structure, axial element.

[22] J. H. G. M. van Beek. Adenine nucleotide-creatine-phosphate module in myocardial metabolic system explains fast phase of dynamic regulation of oxidative phosphorylation. Am J Physiol Cell Physiol, Vol. 293, No. 3, pp. C815–829, 2007.

[23] M. Pasek, J. Simurda, C.H. Orchard, and G. Christe. A model of guinea-pig ventricular myocyte incorporating a transverse-axial tubular system. Prog Biophys Mol Biol, Vol. 96, pp. 258–280, 2008.

[24] Clive Orchard and Fabien Brette. T-tubules and sarcoplasmic reticulum function in cardiac ventricular myocytes. Cardiovascular Research, Vol. 77, No. 2, pp. 237–244, 2008.

[25] Klaus W. Linz and Rainer Meyer. Control of l-type calcium current during the action potential of guinea-pig ventricular myocytes. The Journal of Physiology, Vol. 513, No. 2, pp. 425–442, 1998.

[26] Jinglin Zeng, Kenneth R. Laurita, David S. Rosenbaum, and Yoram Rudy. Two components of the delayed rectifier k+ current in ventricular myocytes of the guinea pig type : Theoretical formulation and their role in repolarization. Circ Res, Vol. 77, No. 1, pp. 140–152, 1995.

[27] Thomas R. Shannon, Fei Wang, Jose Puglisi, Christopher Weber, and Donald M. Bers. A mathematical treatment of integrated ca dynamics within the ventricular myocyte. Biophysical Journal, Vol. 87, No. 5, pp. 3351–3371, 2004. 0006-3495.

[28] J. A. Negroni and E. C. Lascano. A cardiac muscle model relating sarcomere dynamics to calcium kinetics. J Mol Cell Cardiol, Vol. 28, No. 5, pp. 915 – 929, 1996.

[29] S. Matsuoka, N. Sarai, H. Jo, and A. Noma. Simulation of atp metabolism in cardiac excitation-contraction coupling. Prog Biophys Mol Biol, Vol. 85, pp. 279–299, 2004.

[30] T. N. Andrienko, E. Picht, and D. M. Bers. Mitochondrial free calcium regulation during sarcoplasmic reticulum calcium release in rat cardiac myocytes. J Mol Cell Cardiol, Vol. 46, No. 6, pp. 1027 – 1036, 2009.

[31] Ranjan K. Dash and Daniel A. Beard. Analysis of cardiac mitochondrial Na^+-Ca^{2+} exchanger kinetics with a biophysical model of mitochondrial Ca^{2+} handing suggests a 3: 1 stoichiometry. J Physiol, Vol. 586, No. 13, pp. 3267–3285, 2008.

[32] E. Carafoli. Intracellular calcium homeostasis. Annu Rev Biochem, Vol. 56, pp. 395–433, 1987. 0066-4154 (Print) 0066-4154 (Linking) Journal Article Review.

[33] B. O'Rourke and L.A. Blatter. Mitochondrial ca^{2+} uptake: Tortoise or hare? J Mol Cell Cardiol, Vol. 46, pp. 767–774, 2009.

[34] D. E. Wingrove and T. E. Gunter. Kinetics of mitochondrial calcium transport. ii. a kinetic description of the sodium-dependent calcium efflux mechanism of liver mitochondria and inhibition by ruthenium red and by tetraphenylphosphonium. Journal of Biological Chemistry, Vol. 261, No. 32, pp. 15166–15171, 1986.

[35] K. E. Coll, S. K. Joseph, B. E. Corkey, and J. R. Williamson. Determination of the matrix free ca^{2+} concentration and kinetics of ca^{2+} efflux in liver and heart mitochondria. Journal of Biological Chemistry, Vol. 257, No. 15, pp. 8696–8704, 1982.